NASA Technical Memorandum 85644

NASA-TM-85644 19830018746

SLOW CRACK GROWTH IN SPINEL IN WATER

Stephan Schwantes and Wolf Elber

May 1983

NASA
National Aeronautics and
Space Administration

Langley Research Center
Hampton, Virginia 23665

SLOW CRACK GROWTH IN SPINEL IN WATER

Stephan Schwantes* and Wolf Elber
NASA Langley Research Center
Hampton, Virginia 23665

SUMMARY

Magnesium aluminate spinel ($MgAl_2O_4$) was tested in a water environment at room temperature to establish its slow crack-growth behavior. Ring specimens with artificial flaws on the outside surface were loaded hydraulically on the inside surface. The time to failure was measured. Various precracking techniques were evaluated and multiple precracks were used to minimize the scatter in the static fatigue tests. Statistical analysis techniques were developed to determine the strength and crack velocities for a single flaw. Slow crack-growth rupture was observed at stress intensities as low as 70 percent of K_c. A strengthening effect was observed in specimens that had survived long-time static fatigue tests.

INTRODUCTION

Spinel is a ceramic material with strength properties suitable for high-temperature structural applications. Like all ceramics, its fracture toughness is much lower than most structural materials. Studies of fracture toughness and the possibility of environmentally-induced slow crack growth represent a large portion of research in glasses and ceramics today. In the ceramics literature slow crack-growth tests under constant applied stress (ref. 1) are referred to as "static fatigue" tests, and crack-growth tests under monotonically increasing stress or cyclic stress are referred to as "dynamic fatigue" tests.

Like metals, many ceramics display slow crack growth in static fatigue tests in water or water vapor, and display a threshold stress intensity below which cracks apparently will not grow. Much of this work on environmental effects has been done

*DAAD guest student, George Washington University.

on glass (ref. 2), magnesia (ref. 3), and alumina (ref. 4). These materials have three different basic structures: glass is amorphous; magnesia has a cubic crystal structure; and alumina has a hexagonal structure.

Spinel, the material in this study, has a cubic lattice structure like magnesia. The cubic structure is responsible for the existence of plasticity at elevated temperatures (refs. 5 and 6) and the observed microplasticity at room temperature (ref. 7). But dislocation movement, normally associated with plasticity in metals, has not been found in microscopic studies (ref. 8).

The polycrystalline spinel can be produced by sintering or hot-pressing alumina and magnesia powder. First test results in the literature were conducted on non-stoichiometric spinels (refs. 8 and 9). Stoichiometric spinels, which require a precise ratio of fine-grained powder constituents, were first produced and tested in the 1960's. To study slow crack-growth behavior of spinel in water, the specimens need to be precracked. When the constituents are extremely pure and the resultant spinel is dense, it will be transparent. The material in this study was white and translucent, but not transparent. In transparent materials even small cracks of 200 μm depths can be measured by optical methods. But in the material tested crack depths cannot be measured optically and electron microscopy of the fracture surface does not delineate the region of slow crack growth from the region of fast crack growth. In this study crack size was therefore always calculated.

Several precracking techniques were evaluated. Even the most repeatable of these required the use of multiple flaws in each specimen to reduce the scatter in the measured times to failure. Extreme value statistics methods were developed to evaluate the crack-growth rate function. This paper presents the methods and test results.

SYMBOLS

a	crack size parameter, for surface flaws the depth of the crack, m
a_c	critical crack size, m
a_i	initial crack size, m
$a_{c,j}$	critical crack size for the jth load level ($K = K_c$), m
$a_{i,j}$	crack size related to the ith interval in stress intensity and the jth load level, m
b	specimen width, m
c	half surface crack length of surface flaws, m
c_m	critical half surface crack length, m
c_o	initial half surface crack length, m
F_S	correction for stress-intensity function
f_w	finite-width correction
f_ϕ	correction to calculate a stress-intensity value at point of the crack front characterized by the angle ϕ
g	correction of a/t ratio ϕ interactions
K	stress-intensity factor, $N \cdot m^{3/2}$
K_c	critical stress-intensity factor, or fracture toughness, $N \cdot m^{3/2}$
K_{th}	threshold stress intensity, $N \cdot m^{3/2}$
N	number of samples in one distribution
n	exponent for crack-growth power law
M_i	correction factors in the stress-intensity formula
m	number of independent events in the extreme value statistic
$P(x)$	cumulative probability of all events smaller than x
$\bar{P}(x)$	cumulative probability expression in numerical approach for all events smaller than x
$p(x)$	probability density of event x
$\bar{p}(x)$	probability of the interval containing x
$p_m(x)$	probability density of the extreme value x out of m independent events

Q	elliptic integral of the second kind
S	fatigue stress, $N \cdot m^2$
S_i	strength of specimen with i indentations, $N \cdot m^2$
$\bar{S}_i$	mean strength of specimens with i indentations, $N \cdot m^2$
T	time to failure, sec
t	time, sec
$t_{i,j}$	time required to pass the ith stress-intensity intervals at the jth load level, sec
v_i	average crack velocity value for the ith stress-intensity interval, m/sec
Y	correction factor for single-edge notch stress-intensity function
α	constant factor in crack-growth power laws
γ	fraction of the critical crack length
σ_i	standard deviation of the distribution of i indentation specimen
ϕ	elliptical angle

EXPERIMENTAL PROCEDURE

Material

The material tested is nearly pure, dense, and stoichiometric spinel. To meet the requirements of a residual stress-free material for some precrack techniques, a heat treatment was necessary. The annealing process was 24 hours at 1700 K, followed by a slow cool-down with a maximum rate of 25 K per hour. As a result, the average grain size increased slightly from 20 to 25 μm, but some grains had grown to the extreme value of about 100 μm. A typical grain distribution is shown in figure 1. This was followed by an X-ray diffraction analysis to detect residual alumina or magnesia. None was found, indicating the material was stoichiometric. In addition, a chemical analysis was performed. The impurity contents are given in the following table:

Chemical	Impurities, %
Li	0.06
Si	.05
Ca	.03
Fe	.01
Ga	.01

For these small concentrations, only silicon exhibits a tendency to form glassy second phases at very large grains; the metal ions should stay in the bulk. An optical and electron microscope examination was made for second-phase particles. This was performed both at the exterior and on interior fracture surfaces. No indices for second phases like rounded grain edges, different colored areas on polished surfaces, or actual second-phase particles were detected. Figure 2 shows a typical fracture surface. An expanded view of the fracture surface showing "clean" grain boundaries is shown in figure 3. A few pores were in the material as shown in figure 4.

Specimen Preparation

Ring specimens were cut from sintered tube material. The specimens were ground on all surfaces but were not optically flat. High accuracy of all dimensions was necessary for this type of load mechanism. This leads to a high uniformity of the specimens.

Three different types of artificial flaws were tested: saw cuts (ref. 14), and indentation marks with Knoop (ref. 15) and Vickers (refs. 16 to 24) microhardness testers. Artificial flaws were introduced to achieve known and reproducible stress intensities. The flaws are exposed to the environment.

The saw cuts, produced by a 0.15-mm-thick diamond saw blade, were 0.50 mm deep and easy to control. However, the initial notch tip is then rounded and has no singularity. The singularities develop rapidly as a sharp crack starts to grow at

the tip of the notch. This short distance, where the stress intensity increases rapidly, makes this type of specimen unsuitable for slow crack-growth tests. Such specimens were only used for toughness measurements.

The Knoop indenter did not produce a useful flaw for this material. The crack pattern was mostly parallel to the surface. No mean radial crack was achieved. There was substantial chip-off of material within the indentation mark.

The Vickers pyramid indenter did produce a useful flaw for this material. Unfortunately, the resulting crack pattern was neither as simple nor as reproducible as the crack patterns found elsewhere in the literature (refs. 16 and 20 to 24). There were a large number of radial cracks. The lateral cracks parallel to the surface lying under the indentation zone were similar in size to the radial cracks and probably caused the chip-off of material around the indentation mark at the tests. Several load levels of the indenter were tested to check the reduction in strength due to indentations. A load of 25 N was found as the best value and used in all tests. (A brief introduction in indentation techniques is given in appendix A.)

Test Equipment

The specimens were loaded hydraulically through a thin rubber bladder. The specimen holder is shown in figure 6. The ring arrangement was chosen so as to achieve nearly uniform hoop tensile stresses in the specimen (ref. 25). Also, since no grips or bending pins are used, surface damage is avoided. The hydraulic pressure was produced by a hand pump or a power system through an intensifier. A dead weight system held the pressure mechanically constant. For long-time tests, a closed-loop controller was used to maintain a stable pressure. For short-time strength tests, a function generator was used to raise the pressure at a uniform rate to failure stress. This constant ramp was also used to reach the stress levels of the long-time tests. The load and time were recorded for each test. A block diagram for the setup is given in figure 7.

Test Environments

Two different environments were used here--dry nitrogen and distilled de-ionized water. Dry nitrogen was used as an inert environment that should not induce slow crack growth. A wider second ring was placed to seal the specimen from the atmosphere. The interior of the test cell was flushed with a stream of dry nitrogen. When the tests were run in water, a rubber mask was used to seal the space around the specimen. The water in that space was motionless. New fluid was used for each new specimen. Both environments were applied for 10 minutes before the specimens were loaded.

Test Procedure

For the short-time tests, the specimens were loaded with a constant load rate of 170 MPa/s until failure. For the long-time tests, the specimens were loaded at the same rate until the desired pressure was reached. At that point, the time count was initiated. The pressure was maintained at a constant value by the controller either until the specimen failed or the maximum test time (between 10^5 and 10^6 seconds) was reached. If the specimen survived, usually a second ramp increased the stress to failure.

In order to study the influence of long-time testing on the residual strength, 10 specimens were stressed for 24 hours at the lower stress level used here (59 MPa). Half were then fractured directly after this treatment. The second half were placed for an additional period of 24 hours in a water bath and were then tested with the usual short-time test procedure. Some toughness measurements were also made using the short-time test procedure.

ANALYSIS

Existing work in slow crack-growth determination has been done on materials and samples where the crack growth could be measured directly (ref. 2) or in which the

standard precracking techniques led to very uniform initial crack sizes (refs. 20 to 24). In the material under study here, no direct measurement was possible and the same precrack techniques led to significant variability in the initial notch size. Therefore, multiple precracks were used. Analyses were developed to work with these multiple precracks, the longest of which will result in failure. Extreme value statistics concepts are presented in this section for this purpose.

In other previous work (ref. 16), stress intensities due to indentations were considered to be the result of both the remotely applied stress and a residual stress field left by the indentation process. The parameters for the residual stress field were obtained on "dummy" indentations, which are multiple indentations, but so close together that only one causes the failure. The size of the surviving indentation marks contains the needed information. Linear superposition of the residual stress field and the applied stress was used for calculations.

In this study the variability of the notch sizes prevents a similar growth of all notches until fast fracture occurs, so no information could be extracted from the surviving notches.

Normally, the residual stress field is established by a small volume of material around the indentation mark. It acts as a wedge, opening the radial cracks. But in this material, the chip-off surrounding the indentation mark occurred very often, which eliminated the residual stress field. So the stress intensities were calculated here without any account of the residual stresses. A stress-intensity factor formula for a surface crack of elliptical shape (ref. 26) was used. This relation is discussed in appendix B.

Most published research of crack-growth rates uses a power law representation in terms of the stress-intensity factor (ref. 27). While such a power law may fit the test data over some range of stress intensities, deviations are expected both at the growth limit (threshold) and near the fracture. In this study, therefore, a

numerical method for describing the crack-growth rate was developed to obtain the best representation for the "tails" of the crack-growth curve.

Extreme Value Analysis for Multiple Notches

When a specimen contains more than one flaw, the failure will occur at the worst flaw. If the strength distribution for a single flawed specimen is assumed to be known with a probability density function $p_1(S)$, then the probability density function for the lowest strength governed by the worst of m flaws is

$$p_m(S) = m\left[1 - P_1(S)\right]^{m-1} p_1(S)$$

where $P_1(S)$ is the cumulative probability function for the strength of one flaw (ref. 28).

If the distribution $p_i(S)$ is a Gaussian distribution with a mean of $\bar{S}_1$ and a standard deviation σ_1, the calculation of $p_m(S)$ must be performed numerically. The details of the calculation scheme are given in appendix C.

The results show that for four flaws, the strength distribution estimators are

$$\bar{S}_4 = \bar{S}_1 - 1.03\,\sigma_1$$

$$\sigma_4 = 0.70\,\sigma_1$$

and for 32 flaws

$$\bar{S}_{32} = \bar{S}_1 - 2.07\,\sigma_1$$

$$\sigma_{32} = 0.49\,\sigma_1$$

If data exist for specimens with multiple flaws, the above equation pairs can be used to obtain the strength distribution estimators for specimens with single flaws.

Analytical Crack-Growth Rate Analysis

Because the slow crack-growth tests were carried out in environmental chambers with no access to the cracks, and because crack lengths are difficult to measure, the

analysis of crack-growth rate must be performed without knowledge of the crack length as a function of time. This is possible as long as the functions of the stress intensity $K(a)$ and the fracture toughness are known. Two methods can be used: (1) the mathematically constrained growth law method and (2) the unconstrained numerically-derived growth law method. Both methods use the assumption that in a fast fracture test in these brittle materials there is very little crack growth. This fact can still be incorporated in the analysis by assuming that the growth in the short-time tests is a small fraction γ of the critical crack length, so that the initial crack length is given as

$$a_i = (1 - \gamma)a_c$$

where γ is a small number and assumed in this study to be $\gamma = 0.02$.

The critical crack depth for the short-time tests is based on the literature value of critical stress intensity (ref. 26)

$$a_c = \frac{K_c^2 Q}{S^2 F_S^2 \pi}$$

Mathematically Constrained Crack-Growth Law

Beyond the assumption that the slow crack-growth rate is determined only by the stress intensity K, it can be assumed to be constrained by one of the following mathematical laws:

$$\frac{da}{dt} = \alpha\left(\frac{K}{K_c}\right)^n \tag{1}$$

or

$$\frac{da}{dt} = \alpha\left(\frac{K - K_{th}}{K_c}\right)^n \tag{2}$$

Both of these functions can be integrated to obtain the time required to grow from an initial crack depth a_i to a critical crack depth a_c.

For the two-parameter crack-growth law (eq. (1)), the expression for the time to failure is

$$T = \frac{Q^{n/2} K_c^n}{S^n \left(1 - \frac{n}{2}\right) \pi^{n/2} F_S^n \alpha} \left(a_c^{(1-n/2)} - a_i^{(1-n/2)} \right)$$

The two parameters α and n can then be determined to obtain the best fit to all of the test data.

For the three-parameter growth law (eq. (2)), the expression for the time to failure is

$$T = \frac{1}{\alpha} \int_{a_i}^{a_c} \frac{K_c^n \, da}{\left(S \sqrt{\frac{\pi a}{Q}} F_S - K_{th} \right)^n}$$

Numerical integration showed that the above equation is approximately log-linear for median times to failure and asymptotically approaches the threshold stress-intensity factor. The threshold stress-intensity factor can be determined from the long life or runout test data, and the other two parameters α and n can again be determined to provide the best fit to the long-term data.

Unconstrained Numerical Analysis

This method places no mathematical constraints on the crack-growth law and provides a numerical crack-growth law with as many points as there were stress levels in the test program. The method is based on the fact that if the growth rate is only a function of the stress intensity, then in any stress-intensity interval the growth rate is the same and is independent of the stress level.

Figure 8 is a schematic representation of the crack length as a function of the highest three stress levels in the test program. At stress level S_o, the critical

crack length is defined as $a_{c,o}$, and the initial crack length is called a_i. The vertical dashed line indicates that all a_i are assumed equal. The rightmost dashed line is the locus of the critical crack lengths for all stress levels. The second dashed curve makes the lower limit of the higher stress-intensity band; it passes through a_i at the stress level S_o.

If the crack took a finite time to grow from a_i to $a_{c,o}$ in the short-time strength test, then the velocity in that stress-intensity interval is given as

$$V_o = \frac{a_{c,o} - a_i}{T_o}$$

At all lower stress levels the crack will grow at that velocity in the crack length intervals from $a_{1,i}$ to $a_{c,i}$, which are inside this stress-intensity band.

At the stress level S_1, the log mean time to failure is T_1, and the portion of time required to grow through the interval $a_{1,1}$ to $a_{c,1}$ is

$$t_{1,1} = \frac{a_{c,1} - a_{1,1}}{V_o}$$

so that the time required for the crack to grow from a_i to $a_{1,1}$ is

$$t_{2,1} = T_1 - t_{1,1}$$

and the velocity in that (second) stress-intensity interval is

$$V_1 = \frac{a_{1,1} - a_i}{T_1 - t_{1,1}}$$

At stress level S_2, the velocities for the highest two stress-intensity intervals are now known, so that the time required to grow from a_i to $a_{2,2}$ is

$$t_{3,2} = T_2 - \frac{a_{c,2} - a_{1,2}}{V_o} - \frac{a_{1,2} - a_{2,2}}{V_1}$$

and the velocity is then

$$V_2 = \frac{a_{2,2} - a_i}{t_{3,2}}$$

This method is then expanded into a matrix scheme and continued through all stress levels.

The reverse calculation of time to failure as a function of stress levels will provide a function satisfying the initially observed log-mean failure times at all stress levels.

RESULTS AND DISCUSSION

Precrack Technique Evaluation

The strength results of all short-time tests will be presented in terms of probability of failure at a given stress. The probability assigned to the ith data point of N samples is

$$P_i = \frac{i - 1/2}{N} \qquad (i = 1, \ldots, N)$$

To confirm the literature value of critical stress intensity (ref. 11), a series of ring specimens were tested with narrow sawcuts across the full width of the specimen. Four conditions were chosen:

1. Specimen annealed first, then cut and tested in water.
2. Specimen annealed first, then cut and tested in dry nitrogen.
3. Specimen cut first, then annealed and tested in dry nitrogen.
4. Specimen not annealed, cut and tested in dry nitrogen.

Figure 9 shows the distributions of critical stress intensities for tests under these four conditions. For the notch-tip radius r resulting from the saw blade of 0.15 mm thickness, the following correction for the stress intensity was taken from the literature (ref. 14):

$$K = \text{Corr} \cdot SY\sqrt{a}$$

$$Y = 1.99 - 0.41\left(\frac{a}{t}\right) + 18.7\left(\frac{a}{t}\right)^2 - 38.48\left(\frac{a}{t}\right)^3 + 53.85\left(\frac{a}{t}\right)^4$$

Corr = 0.75 for 0.15 mm width

These data indicate that the water environment reduced the critical stress intensity about 20 percent below the value for dry nitrogen.

Annealing the specimen after saw cutting resulted in a critical stress intensity about 20 percent higher than those tests where the specimens were not annealed after cutting.

Tests on the material as received resulted in the lowest critical stress intensities in dry nitrogen.

Annealing changes the grain size and reduces residual stresses. These tests provide no definite insight into whether the smaller grain material has a lower toughness or whether the reduction of residual stresses causes an apparent increase in toughness.

For the long-time tests in water, the critical stress intensity for the spinel was taken to be

$$K_c = 1.90 \text{ MPa}\cdot\text{m}^{1/2}$$

As stated earlier, the rapid rise in stress intensity in the sawcut specimens makes them unsuitable for slow crack-growth tests. For these tests, the indentation technique, using the Vickers standard microhardness indenter, was applied. The specimens with four indentations were used to obtain crack size data from nonfailed indentations ("dummy" indentations (ref. 16)), but the observation of ill-defined and nonsimilar crack patterns and different strength values led to the use of multiple notches to reduce the scatter. Four test conditions were used to assure that the

indentation technique resulted in a significant reduction in the short-time strength. Those conditions were:

1. Without indentations in dry nitrogen (baseline).
2. With four indentations in dry nitrogen.
3. With four indentations in water.
4. With 32 indentations in water.

Figure 10 shows the failure probability distributions for these four conditions. The mean baseline strength was 166 MPa. This strength was reduced to 120 MPa when tested with four indentations in dry nitrogen. In all samples the first fracture occurred at an indentation mark, which showed that the artificial flaws had a dominant size. The strength reduction was acceptable, so the indentation load of 25 N was fixed for the remaining program.

In water the mean strength with 4 indentations was further reduced to 100 MPa, and specimens with 32 indentations had an average strength of 86 MPa as well as a reduced scatter.

Long-Time Tests

The long-time test program was started with single indentations, but the scatter in time to failure made this test program unmanageable. By choosing 4 indentations, a reduction in scatter resulted and 22 long-time tests were run at 6 stress levels. These results are shown in figure 11. The two results plotted at 0.1 s represent failures immediately upon reaching the test stress level. Additional failures during the ramp loading are not plotted as long-time failures. The two tests plotted at $t = 10^6$ s represent specimens which did not fail (runouts). The data have only a slightly visible trend at lower stresses, but no correlation could be found and the data were considered to have too much scatter to obtain crack-velocity estimates.

A second group of 42 specimens was tested with 32 indentations spaced equally around the circumference. The results are shown in figure 12. The data from these

tests are in much closer groups and will be used for the analysis of crack-growth rates.

Calculation of Crack-Growth Rates

The crack-growth calculations in the numerical method were based on the mean critical crack length $\left(a_c = 265\ \mu m\right)$ in the short-time tests as well as on the curve in figure 12, which represents a "smooth" curve fitting the log-mean values of the time to failure data of each stress level. This assures the maximum use of the data.

In figure 13 the solid continuous line represents the results of the numerical crack-growth calculations. It exhibits an S-curve shape with an apparent threshold and a critical stress intensity. The apparent threshold stress intensity was about 73 percent of the critical value. For comparison, the mathematical crack-growth law

$$\frac{da}{dt} = \alpha\left(\frac{K}{K_c}\right)^n$$

was established. This law is represented by the thin continuous line in figure 13. Because of the mathematical constraint, this law is a straight line and does not reflect the apparent threshold of failure, nor the apparent acceleration near fracture. The constants α and n were determined by the procedure explained in the analysis section as

$$\alpha = 5.3 \times 10^{-5}$$

$$n = 38.5$$

In the mathematical law with a threshold singularity

$$\frac{da}{dt} = \alpha\left(\frac{K - K_{th}}{K_c}\right)^n$$

the trend to a threshold is included. This law is shown as the dashed curve in figure 13. The constants were determined as

$\alpha = 7$

$n = 13$

$K_{th} = 0.6\ K_c$

Assessment of Data Scatter

To obtain the best estimate of the distribution of short-time strengths for both the 4 indentation and the 32 indentation specimens, least-squares regressions were performed on each data set, with the test stress as the dependent variable and time to failure as the independent variable. The distributions for the short-time failure strength were then taken as the distribution of test stresses around this trend line.

Starting with the distribution for the 32 indentation specimens, the extreme value analysis was employed to deduce the strength distribution for a single indentation. By reverse calculation, the expected distribution for the four indentation specimens was then deduced.

Figure 14 shows the experimentally obtained strength distributions superimposed on the calculated extreme value distributions. This shows excellent agreement between the expected difference in strength and the observed difference in strength.

The causes of strength scatter can be any of the following:

1. Scatter in effective initial flaw size.
2. Scatter in local fracture conditions (toughness, microstructure).
3. Scatter in critical stress intensity among specimens.

The third cause can be eliminated by the following logic: If all of the scatter was due to specimen-wise variability in K_c, then all flaws on one ring could have the same strength due to the same crack size, so that no strength difference between 4 and 32 indentations would result. If there was significant ring-to-ring variability

in K_c, the reduction in mean between 4 and 32 indentation specimens would be less than predicted.

But the experimental reduction in the mean was precisely as predicted by the extreme value analysis. Therefore, it can be concluded that the ring-to-ring variability in K_c is insignificant. The second cause of scatter--scatter in local fracture toughness--does not explain the scatter trend in the long-time failure. The difficulty here is the estimation of the influence of the changes while a crack is growing. Surely there is a local variation in toughness from grain to grain, but it is not certain how that influences the macroscopic observations.

The best model results from the assumption that the dominant cause of scatter lies in the initial effective crack length. So this model tries to represent all local variations in one parameter.

For the extreme value distribution for short-time strength with 32 notches, an initial crack length distribution for the dominant flaw was derived based on a constant fracture toughness. This distribution is shown in figure 15.

Lifetime values were then calculated for the initial crack lengths, representing 5 percent and 95 percent of the cumulative probability. These data were used for the definition of the expected scatter band for the long-time test results. Figure 16 shows that the test data fall within the expected scatter.

The same confidence band was calculated for the four indentation specimens and, as seen in figure 17, much larger scatter is expected here as was observed.

These data have shown that the variability in initial crack length can explain the variability of the test data. By further deduction it can also be shown that any variability in the crack-growth law must be small in comparison to the effect due to the initial crack length. If a significant variability existed in the crack-growth law, then the time to failure at the lower stress levels would show a variability larger than that deduced on the basis of the scatter in crack length alone. But at all stress levels the time to failure variability is contained in the expected

scatter bands, so that a variability in crack-growth law could not have contributed significantly to the scatter.

Fracture Tests on Runouts

All specimens which did not fail in the long-time tests were fractured by ramp loading to establish their residual strengths. To analyze the obvious increase in residual strength over the short-time strengths, a special test was applied. The baseline short-time fracture specimens had been tested after 10 minutes in water as mentioned previously. Three test conditions were established for these strength tests:

1. Unstressed specimen, 24 hours in water, then tested.

2. Specimen stressed for 24 hours in water at 59 MPa, then tested by continuing the ramp test.

3. Specimen stressed for 24 hours in water at 59 MPa, then 24 hours unstressed in water, then tested to failure in the usual short-time manner.

In figure 18 the strength distributions from these tests show that the 24 hours' unstressed exposure resulted in a small strength increase over the baseline tests run after 10 minutes in water. The specimen exposed under stress for 24 hours had an average strength about 15 percent higher than the baseline tests, independent of whether they were first unloaded, placed in a water bath, or immediately fractured.

Such strengthening under stress has been previously observed but not explicitly reported. Several mechanisms should be considered as the cause for this strengtening. A plastic or viscoplastic blunting under long-term stress might reduce the stress intensity. But the specimens which had been unloaded to possibly reverse such blunting resulted in the same strengths as the specimens failed immediately. This would weaken the plastic blunting argument.

The material is believed to be mildly soluble in water, and the solubility is assumed to increase with stress. This could cause an irreversible blunting

consistent with the data. Microscopic crack branching at very low crack velocities could also effectively cause blunting. This would also be irreversible and consistent with the observation.

CONCLUSIONS

The magnesium aluminate spinel exhibits slow crack growth in water environment at room temperature. It exhibits an apparent threshold level of 73 percent of the fracture toughness, and exposure at stress intensities below that level results in a small elevation of the apparent toughness.

For this material the Vickers indentation precracking method was found to be usable but not ideal. A statistical extreme value analysis was developed to make use of specimens with multiple precracks and to minimize the effects of data scatter on the determination of crack-growth properties.

A numerical method for the determination of crack-growth rate was developed to free the crack-growth law from the artificial mathematical constraints of the normally used power laws.

Logical arguments were used to establish that the specimen-to-specimen variability in fracture toughness was small and that all local variability could be represented in a one-parameter model, varying the crack length to obtain the observed variability in time to failure data.

APPENDIX A

PRECRACK TECHNIQUE WITH VICKERS HARDNESS TESTERS

This technique was introduced by Palmquist (ref. 18), who suggested to use it for qualitative determinations of brittle metals. But the fundamental relations between hardness, crack length, and fracture toughness were unknown. So he only measured the crack length at the corners of the indentation marks to rank different materials. The next step was the observation of the residual stresses, which influence the resulting crack length (ref. 17).

A breakthrough was made by applying fracture mechanics to that problem, which allowed the calculation of fracture toughness from the indentation crack pattern (ref. 20). A lot of emphasis was given to the study of the details of the fracture process, and the technique is frequently used for precracking, especially in glass materials.

A short description will be given of what happens during the indentation process.

1. Under the indenter tip, a (plastic) deformation zone develops. Its dimension is only slightly larger than the contact area between surface and indenter (ref. 19).

2. While applying the load, a crack pattern of two intersecting penny-shaped cracks starts to grow directly under this plastic zone.

3. At the maximum load, the maximum pentration is reached. The cracks have a circular shape, they are completely embedded, and they are perpendicular to each other.

4. While unloading the indenter, these cracks break through to the surface. Their shapes then become semicircular.

5. Under the plastic zone, an additional "lateral" crack pattern develops. These cracks are parallel to the surface, in contrast to the earlier mentioned radial cracks which are perpendicular to the surface.

This can only be observed in ideal materials such as glass and fine grain ceramics. The result of the process should be a crack pattern of reproducible dimensions as shown in figure A1.

It is obvious that this method must leave residual stresses in the specimen. The plastic zone acts as a compressed spring so that at the outer crack front, tensile stresses are present.

If the material shows slow crack growth in special environments, an increase of the surface crack length c_o can be observed. This can shift the initial crack size to c_o', which is somewhat larger than c_o.

For the calculation of the stress-intensity factor, the residual stresses are taken into account in the literature (ref. 16). In those calculations, the total stress intensity is obtained by superimposing residual stresses on the stress intensity due to the remote loading as given by

$$K = \frac{X_r L}{a^{3/2}} + S\sqrt{\pi a}\, F_S$$

where L is the indenter load and X_r is the constant factor. This formula is valid for semicircular crack shapes (a = c). Here, no correction is applied because a crack-opening displacement would decrease the compressive stresses of the plastic zone. The factor X_r is to be determined from observation of a maximum crack length c_m in an inert environment and a short-time test. For this purpose, the "dummy" indentations are used (ref. 16). This maximum crack length is introduced as the maximum stable crack length, with the condition $K = K_c$ and $dK/dc = 0$. From this theory it should be a value with very low scatter. In this study, the cracks had an

undefined pattern and the dimension was scattered in a wide range. Measurements of c_m failed because no crack growth was observed at those indentations which did not cause the failure in short-time tests. If tested in water, the indentation center chipped out for almost every specimen. Because the chipping and the crack size variability violate the basic assumptions of the theory, this microstructure and this material represent a limit for the application of the indentation technique.

APPENDIX B

STRESS-INTENSITY EQUATIONS

The stress-intensity factors for a generalized elliptical surface crack were developed by Newman and Raju (ref. 26). They used a three-dimensional finite-element solution to determine stress intensities for a large number of elliptical configurations, and then developed algebraic fitting functions to express the results in terms of the crack parameters (see fig. B1). The general equation for the stress intensity at a point along the crack front is

$$K_I = S\sqrt{\pi \frac{a}{Q}}\, F_S$$

where Q is the elliptic integral of the second kind and can be approximated as

$$Q = 1 + 1.464\left(\frac{a}{c}\right)^{1.65} \qquad \text{for} \quad a/c \le 1$$

and F_S is the correction function of four parameters, a/c, a/t, c/b, and ϕ. It was expanded into the algebraic form

$$F_S = \left[M_1 + M_2\left(\frac{a}{t}\right)^2 + M_3\left(\frac{a}{t}\right)^4\right] f_\phi g f_w$$

where the functions M_i depend only on the crack-depth-to-length ratio a/c

$$M_1 = 1.13 - 0.09\,\frac{a}{c}$$

$$M_2 = -0.54 + \frac{0.89}{0.2 + \frac{a}{c}}$$

$$M_3 = 0.5 - \frac{1}{0.65 + \frac{a}{c}} + 14\left(1 - \frac{a}{c}\right)^{24}$$

The functions f_ϕ and g are functions to correct point location and crack geometry

$$f_\phi = \left[\left(\frac{a}{c}\right)^2 \cos^2 \phi + \sin^2 \phi\right]^{1/4}$$

$$g = 1 + \left[0.1 + 0.35\left(\frac{a}{t}\right)^2\right](1 - \sin \phi)^2$$

and f_w is the finite-width correction factor

$$f_w = \left[\sec\left(\frac{\pi c}{2b}\sqrt{\frac{a}{t}}\right)\right]^{1/2}$$

For the particular crack configuration, $a/c = 0.8$ was chosen. The stress intensity is essentially constant along the crack front, so ϕ no longer has any influence. Fatigue cracks generally stabilize at that value of a/c and continue to grow with that shape. Then ϕ can be assumed to be $\pi/2$ (evaluated the deepest point) and the calculation is easier.

In this study the ring geometry was

$b = 6.35$ mm

$t = 2.54$ mm

and together with $a/c = 0.8$

$$\frac{c}{b} = 0.8\,\frac{a}{b}$$

the various functions were evaluated as

$M_1 = 1.058$

$M_2 = 0.350$

$M_3 = -0.190$

$Q = 2.013$

$$f_{\phi} = 1$$

$$g = 1$$

$$f_{w} = \left[\sec\left(\pi \frac{a}{1.6b}\sqrt{\frac{a}{t}}\right)\right]^{1/2}$$

so that F_S became a function of a/t and a/b, which was numerically evaluated for each value of a.

APPENDIX C

EXTREME VALUE STATISTICS MODEL

The derivation of probability density functions and cumulative probability functions for multiple flaws is complicated by the fact that the cumulative probability $P(S)$ of a normal distribution can only be obtained numerically. An iterative scheme was therefore developed to obtain these functions for 2, 4, 8, 16, and 32 flaws in turn.

Figure C1 shows a two-dimensional probability domain for the strengths of two flaws, S_1 and S_2. In discrete form, the probability that the strength of the first flaw is within ΔS of S_i is

$$\bar{p}(S_i) = \int_{S}^{S+\Delta S} p(S)\, dS$$

The probability that the weakest of two flaws has strength S within the interval ΔS is the summation of the probability products in the shaded area, which is

$$\bar{p}_2(S_i) = \bar{p}_1^2(S_i) + 2\bar{p}_1(S_i) \sum_{j=i+1}^{N} \bar{p}(S_j)$$

and the cumulative probability function in discrete form for the weakest of two flaws is

$$\bar{p}_2(S_i) = \sum_{j=1}^{i} \bar{p}_2(S_j)$$

This calculation was performed numerically for the unit normal distribution in 200 discrete intervals between -5 and +5. The original discretized distribution was rescaled to assure that

APPENDIX C

$$\sum_{i=1}^{N=200} \bar{p}_i(S) = 1$$

Figure C2 shows the cumulative distributions obtained for 1 through 32 flaws. The mean value for the distribution $\bar{p}_m(S)$ is obtained from

$$\bar{S}_m = \sum_{i=1}^{N=200} \bar{p}_m(S_i) S_i$$

and variance σ_m^2 is obtained from

$$\sigma = \sum_{i=1}^{N=200} \left(S_i - \bar{S}_m\right)^2 \bar{p}_m(S_i)$$

Higher order estimators were not evaluated.

REFERENCES

1. ASTM - Designation E206-64, Section 3.

2. Wiedehorn, S. M.: Crack Growth an an Interpretation of Static Fatigue. Journal of Non-Crystalline Solids, vol. 19, 1975, pp. 169-181.

3. Rhodes, W. H.; Cannon, R. M., Jr.; and Vasilos, T.: Stress-Corrosion Cracking in Polycrystalline MgO. Fracture Mechanics of Ceramics - Volume 2, R. C. Bradt, D. P. H. Hasselman, and F. H. Lange, eds., Plenum Press, 1974, pp. 709-734.

4. Wiederhorn, J. M.: Fracture of Sapphire. Journal of the American Ceramic Society, vol. 52, no. 9, 1969, pp. 485-491.

5. Stewart, R. L.; and Bradt, R. C.: Fracture of Single Crystal $MgAl_2O_4$. Journal of Materials Science, vol. 15, 1980, pp. 67-72.

6. Palmour, H.: Multiple Slip Processes in Magnesium Aluminate at High Temperatures. Proceedings of the British Ceramic Society, no. 6, 1966, pp. 209-224.

7. Palmour, Hayne; Choi, Doug M.; Barnes, L. D.; McBrayer, R. D.; and Kriegel, W. W.: Deformation in Hot-Pressed Polycrystalline Spinel. Materials Science Research - Volume A, H. H. Stadelmaier and W. W. Austin, eds., Plenum Press, 1963.

8. Radford, K. C.; and Newey, C. W. A.: Plastic Deformation in Magnesium Aluminate Spinel. Proceedings of the British Ceramic Society, no. 9, 1967, pp. 131-145.

9. Bansal, G. K.; and Heuer, A. H.: Precipitation in Non-stoichiometric Magnesium Aluminate Spinel. Philosophical Magazine, vol. 29, no. 4, 1974, pp. 709-722.

10. Rice, G. K.; and McDonough, W. J.: Ambient Strength and Fracture Behavior of $MgAl_2O_4$. Proceedings of the International Conference on Mechanical Behavior of Material - Volume 4, The Society of Materials Science, Japan, 1972.

11. Stewart, R. L.; Iwasa, M.; and Bradt, R. C.: Room-Temperature K_{I_c} Values for Single-Crystal and Polycrystalline $MgAl_2O_4$. Journal of the American Ceramic Society, vol. 69, no. 2, 1981, pp. C-22 - C-23.

12. Stewart, R. L.; and Bradt, R. C.: Fracture of Polycrystalline $MgAl_2O_4$. Journal of the American Ceramic Society, vol. 63, no. 11-12, 1980, pp. 619-623.

13. Kanzaki, Shuzo; Naragawa, Zenbe-e; Hamano, Kenya; and Saito, Katsuidi: Effect of Non-stoichiometry on Microstructure and Mechanical Strength of Mg-Al Spinel Ceramics. Kogyo-Kyokai-Shi, vol. 87, no. 5, 1979, pp. 230-237.

14. Pabst, R. F.: Determination of K_{I_c} Factors with Diamond-Saw-Cuts in Ceramic Materials. Fracture Mechanics of Ceramics - Volume 2, R. C. Bradt, D. P. H. Hasselman, and F. H. Lange, eds., Plenum Press, 1974, pp. 555-566.

15. Petrovic, J. J.; and Mendivatto, M. G.: Fracture from Controlled Surface Flaws. Fracture Mechanics Applied to Brittle Materials, S. W. Freiman, ed., ASTM STP 678, 1978, pp. 73-82.

16. Lawn, B. R.; Marshall, D. B.; Austin, G. R.; and Dabbs, T. P.: Fatigue Analysis of Brittle Materials Using Indentation Flaws - Part I. Journal of Materials Science, vol. 16, 1981, pp. 2846-2854.

17. Dawihl, Walter; and Altmeyer, George: Ueber das Verfahren zur Bestimmung des Formaenderungswiderstandes hochwarmfester Werkstoffe, insbesondere von Hartmetallen, durch die Rissbildungsarbeit. (Fracture Strain Energy Release Model for Determining Stiffness of High-Temperature Materials, Particularly High-Temperature Metals.) Zeitschrift fuer Metallkunde, vol. 55, no. 5, 1964, pp. 231-237.

18. Palmgvist, Sven: Rissbildungsarbeit bei Vickers-Eindruecken als Mass fuer die Zaehigkeit von Hartmetallen. (The Use of the Fracture Strain Energy Release Rate During Vickers Hardness Indentation as a Measure of Ductility of High-Strength Metals.) Archiv fuer das Eisenhuettenwesen, vol. 33, no. 9, Sept. 1962, pp. 629-634.

19. Evans, A. G.: Fracture Toughness: The Role of Indentation Technique. Fracture Mechanics Applied to Brittle Materials, S. W. Freimen, ed., ASTM STP 678, 1978, pp. 112-135.

20. Lawn, B. R.; and Swain, L.: Microfracture Beneath Point Indentations in Brittle Solids. Journal of Materials Science, vol. 10, 1975, pp. 113-122.

21. Lawn, B. R.; Marshall, D. B.; and Chantikut, P.: Mechanics of Strength Degrading Contact Flaws in Silicon. Journal of Materials Science, vol. 16, 1981, pp. 1769-1775.

22. Lawn, B. R.; Evans, A. G.; and Marshall, D. B.: Elastic/Plastic Indentation Damage in Ceramics: The Median/Radial Crack System. Journal of the American Ceramic Society, vol. 63, no. 7-8, 1980, pp. 574-582.

23. Austis, G. R.; Chantikul, P.; Lawn, B. R.; and Marshall, D. B.: A Critical Evaluation of Indentation Techniques for Measuring Fracture Toughness: I--Direct Crack Measurement. Journal of the American Ceramic Society, vol. 64, no. 9, Sept. 1981, pp. 533-538.

24. Chautikul, P.; Austis, G. R.; Lawn, B. R.; and Marshall, D. B.: A Critical Evaluation of Indentation Techniques for Measuring Fracture Toughness: II--Strength Method. Journal of the American Ceramic Society, vol. 64, no. 9, Sept. 1981, pp. 539-543.

25. Sedlacek, R.: Tensile Fatigue Strength of Brittle Materials. AFML-TR-66-245, Air Force Materials Laboratory, 1968.

26. Newman, J. C., Jr.; and Raju, I. S.: Stress-Intensity Factor Equations for Cracks in Three-Dimensional Finite Bodies. NASA TM X-83200, Aug. 1981.

27. Rittes, John E., Jr.; and LaPorte, R. P.: Effect of Test Environment on Stress-Corrosion Susceptibility of Glass. Journal of the American Ceramic Society, vol. 58, no. 7-8, 1975, pp. 265-267.

28. Ledermann, Walter: Handbook of Applicable Mathematics - Volume II, Chapter 15. John Wiley - Interscience Publications, 1980.

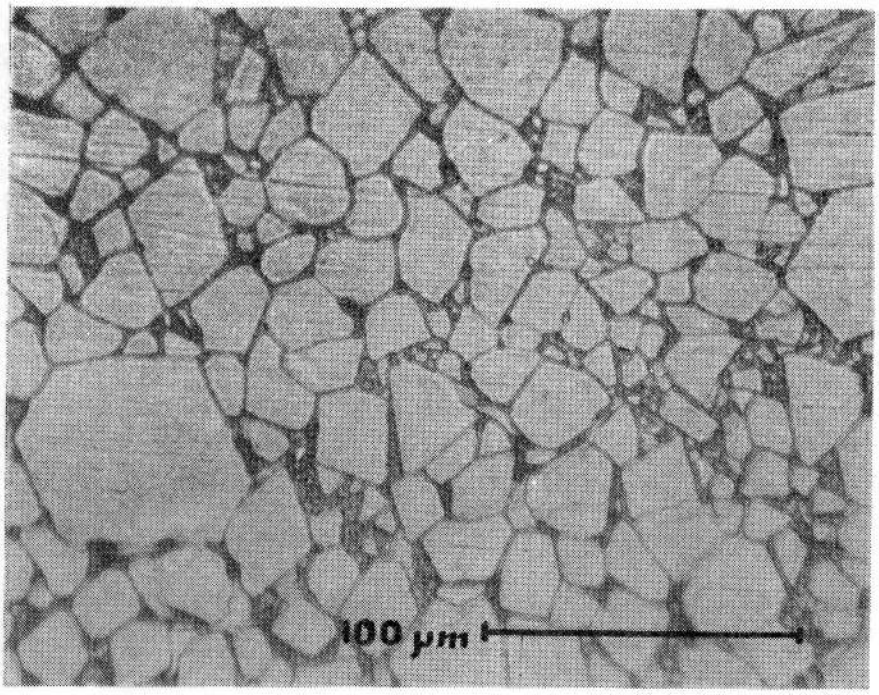

Figure 1. - Grain structure, thermal etched.

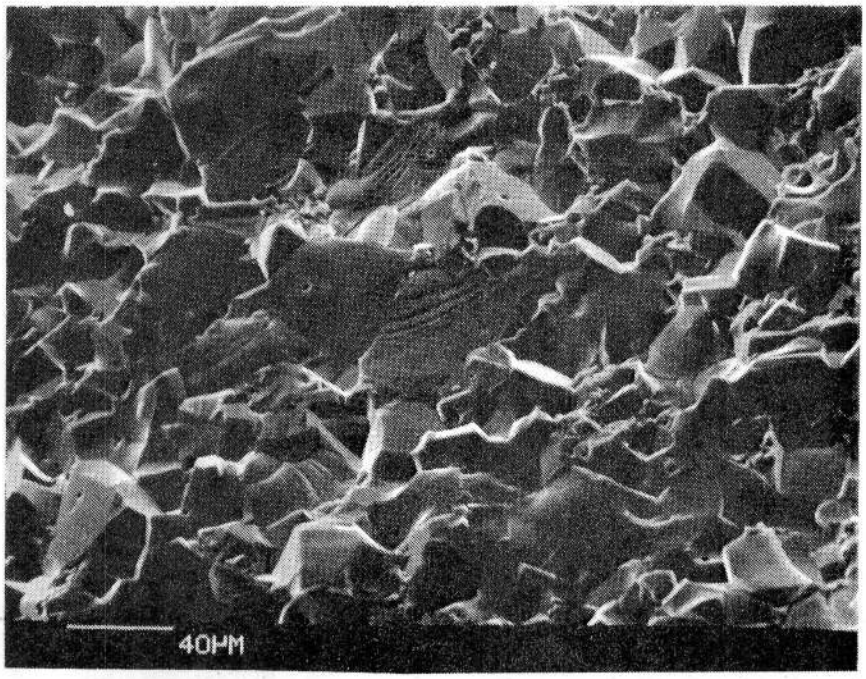

Figure 2. - Fracture surface, overview.

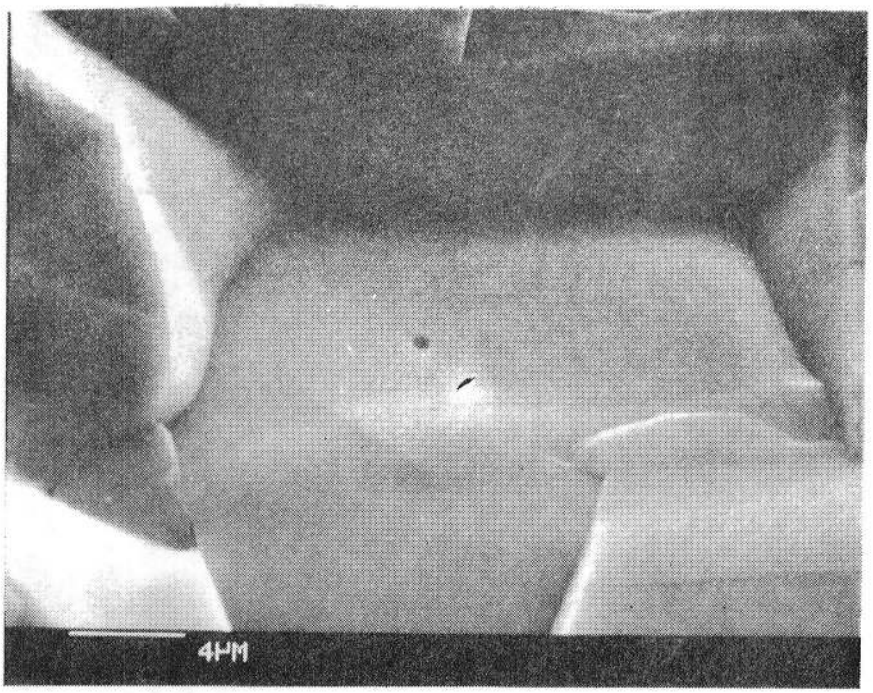

Figure 3. - Grain boundary on fracture surface.

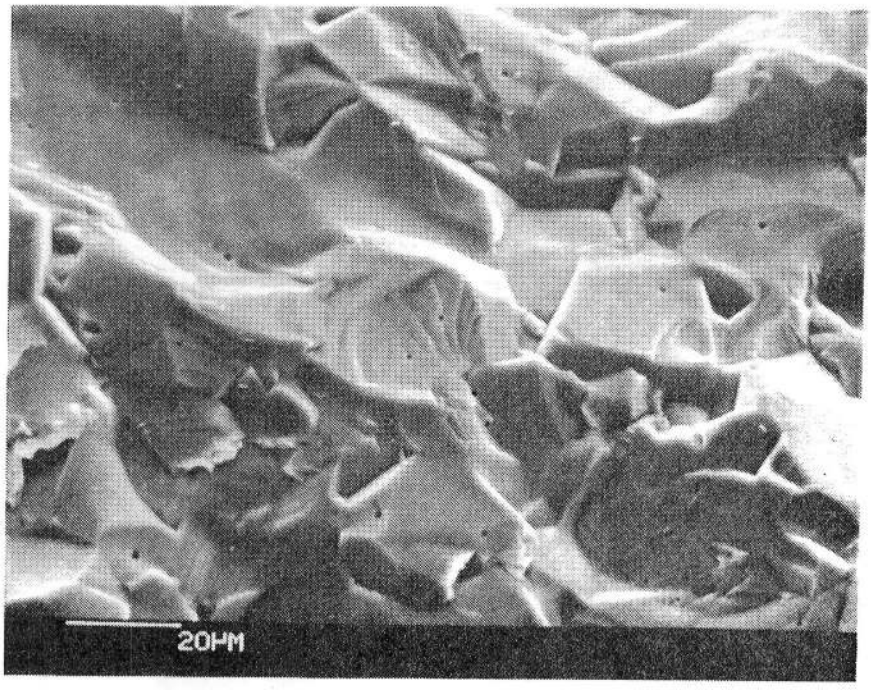

Figure 4. - Details of fracture surface, porosity.

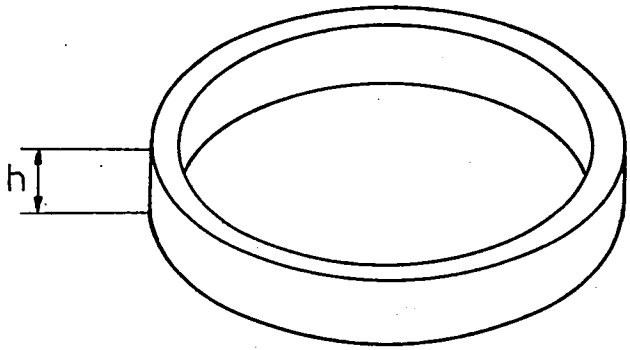

ϕ_{outer}: 55.88 mm
ϕ_{inner}: 50.80 mm
h : 6.35 mm

Figure 5. - Ring specimen with dimensions.

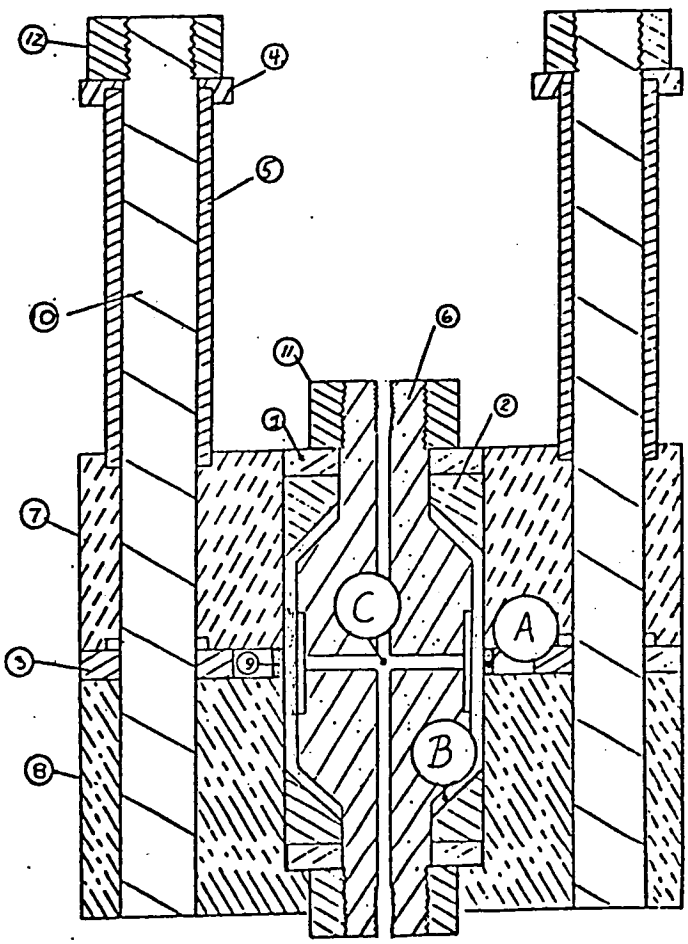

A - RINGSPECIMEN

B - RUBBERBLADDER

C - HYDRAULIC LINE

Figure 6. - Cross section of the loadcell.

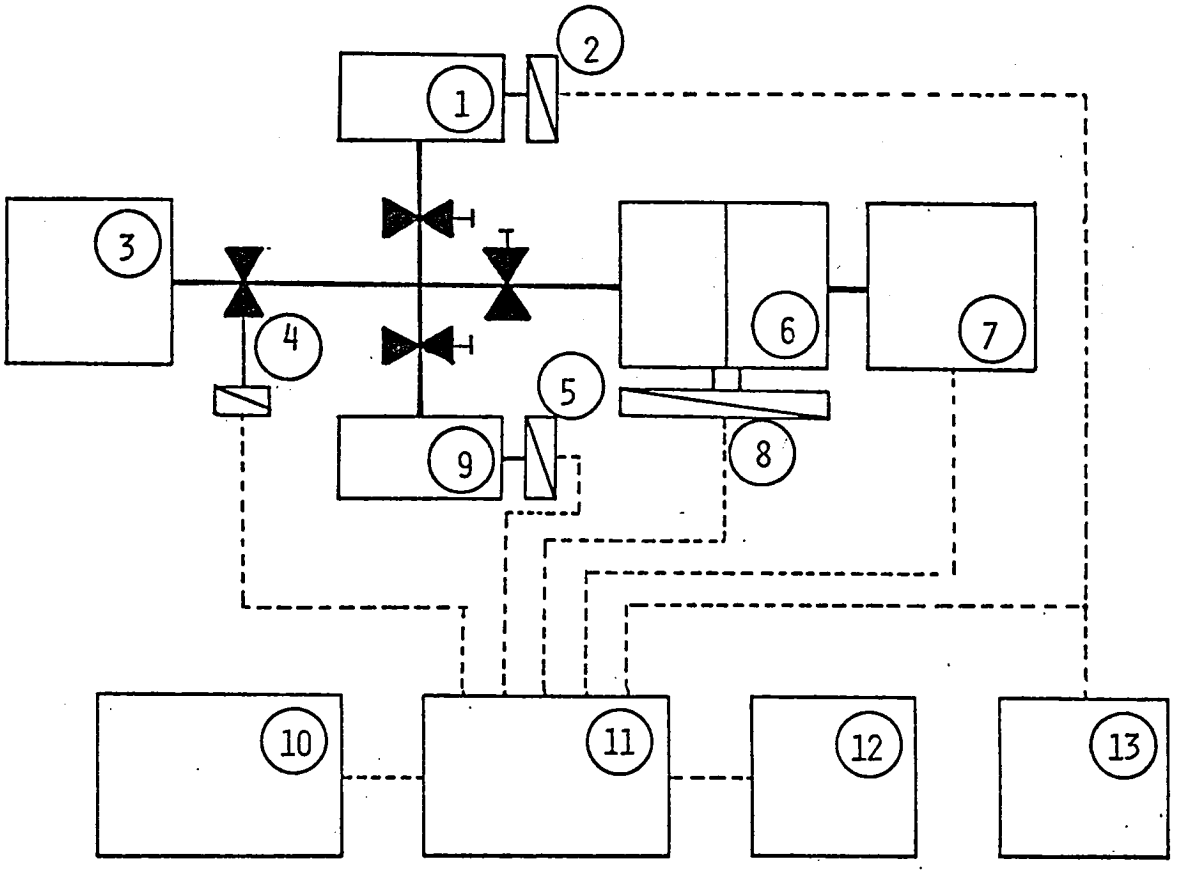

1. Specimen holder
2. Pressure transducer
3. Fluid-tank
4. Solenoid-valve
5. Position-transducer
6. Intensifier
7. Power pump
8. Servo-valve
9. Deadweight and pump
10. Function generator
11. Controller
12. Stop watch
13. Time based recorder

Figure 7. - Blockdiagram of setup.

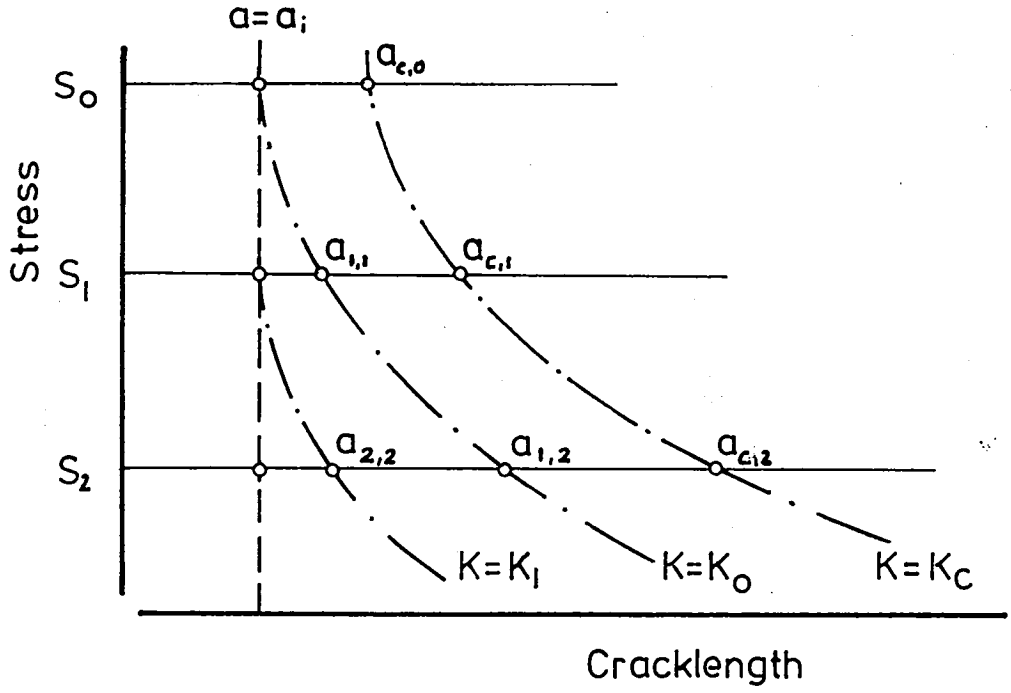

Figure 8. - Relation between crack growth and stress.

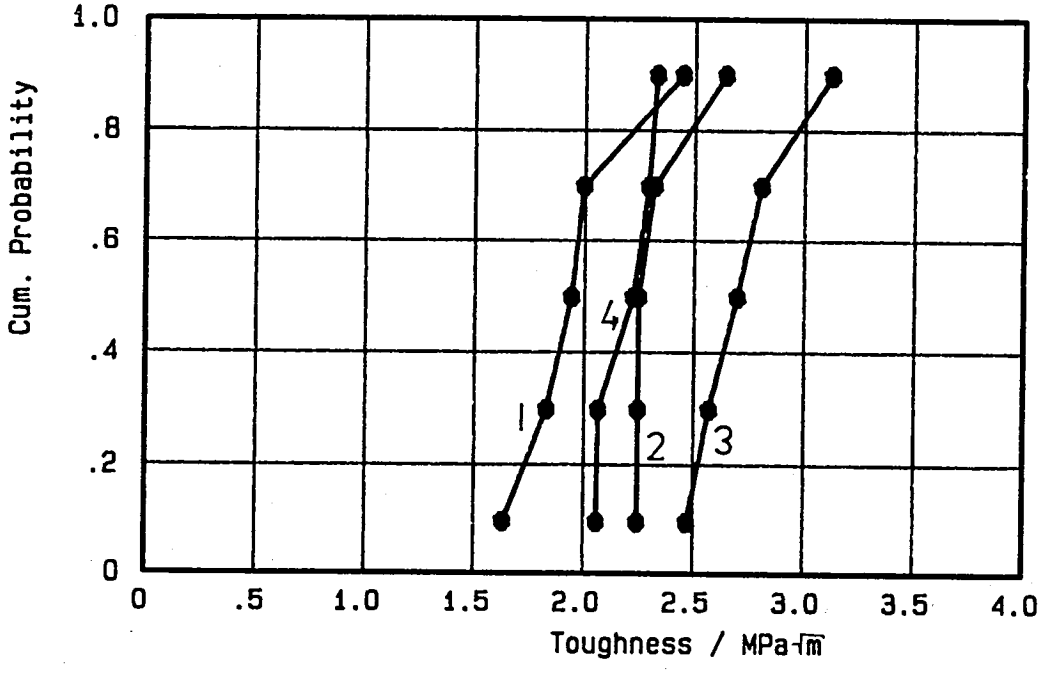

Figure 9. - Fracture toughness data.

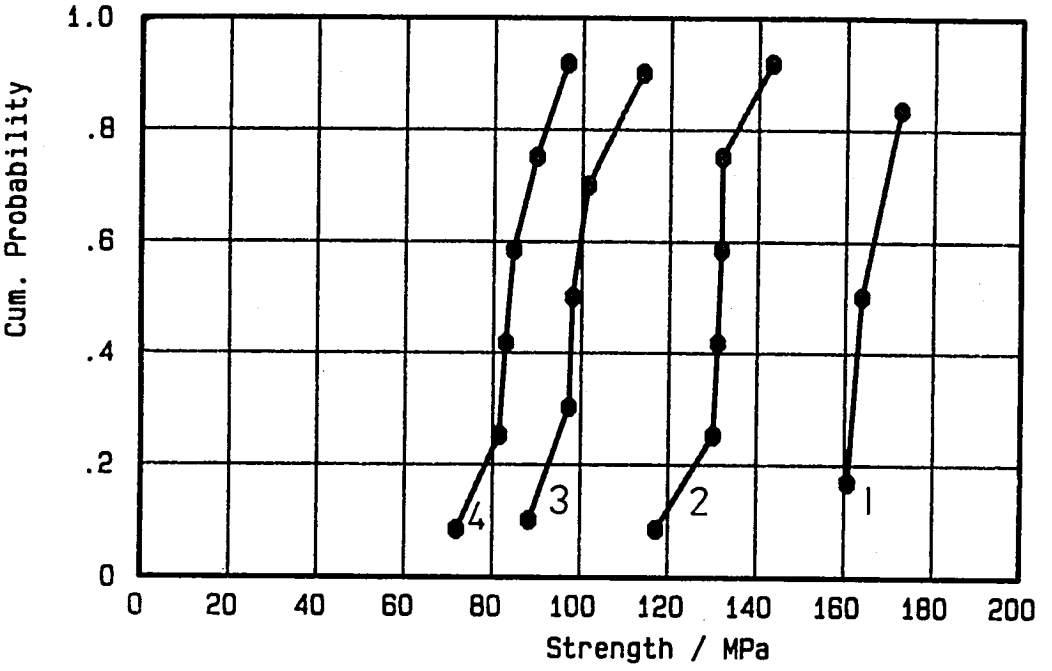

Figure 10. - Short time strength distribution

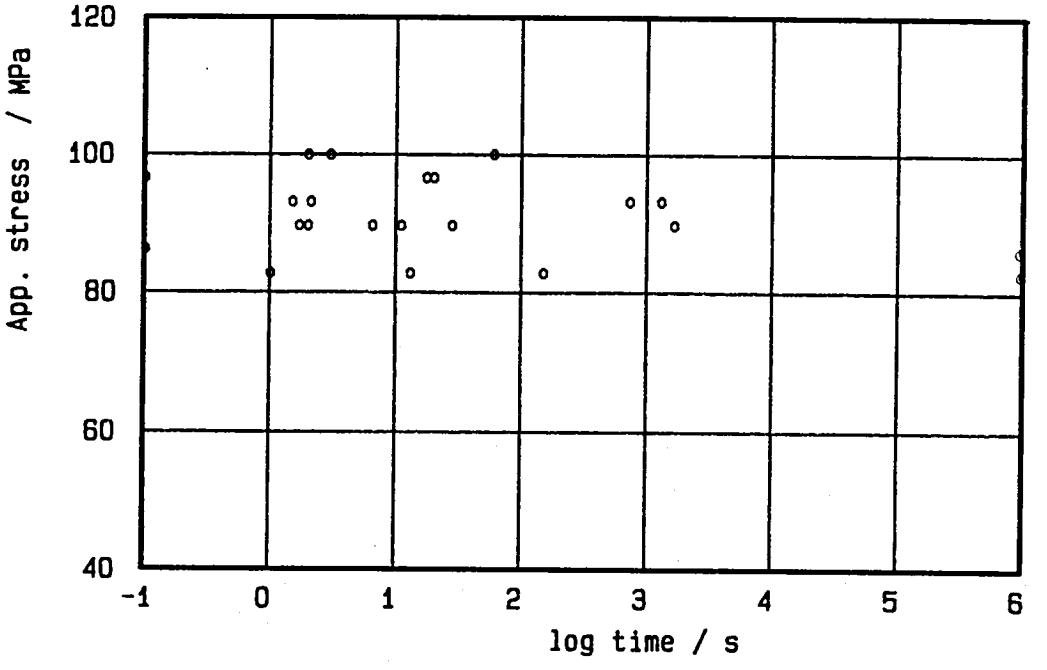

Figure 11. - Time - to - failure data for 4 indentations.

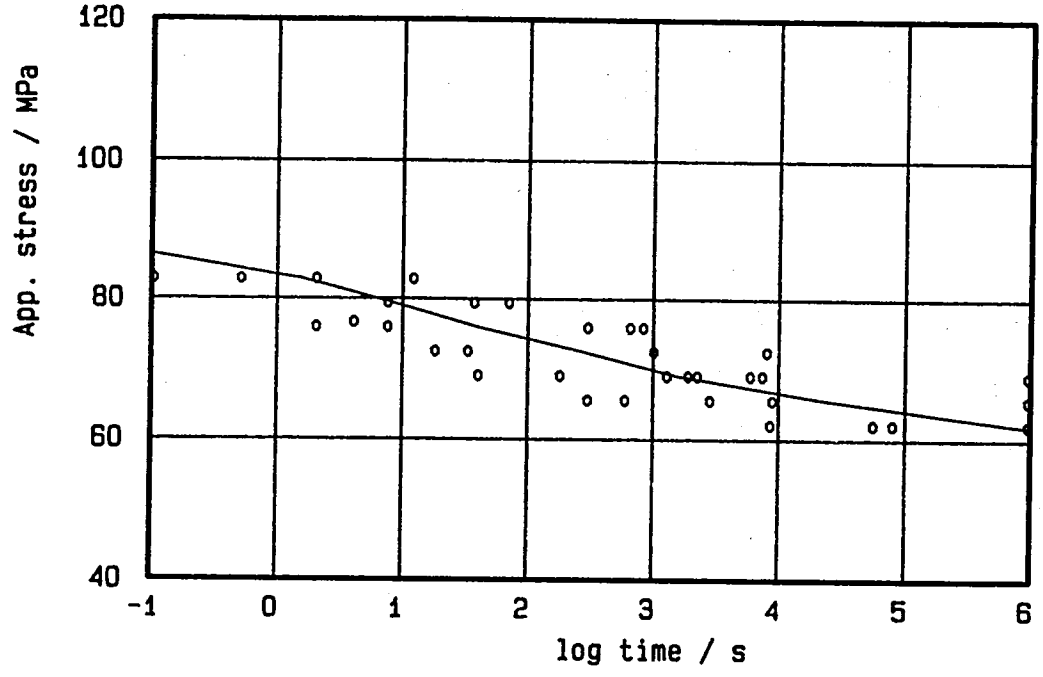

Figure 12. - Time - to - failure data for 32 indentations.

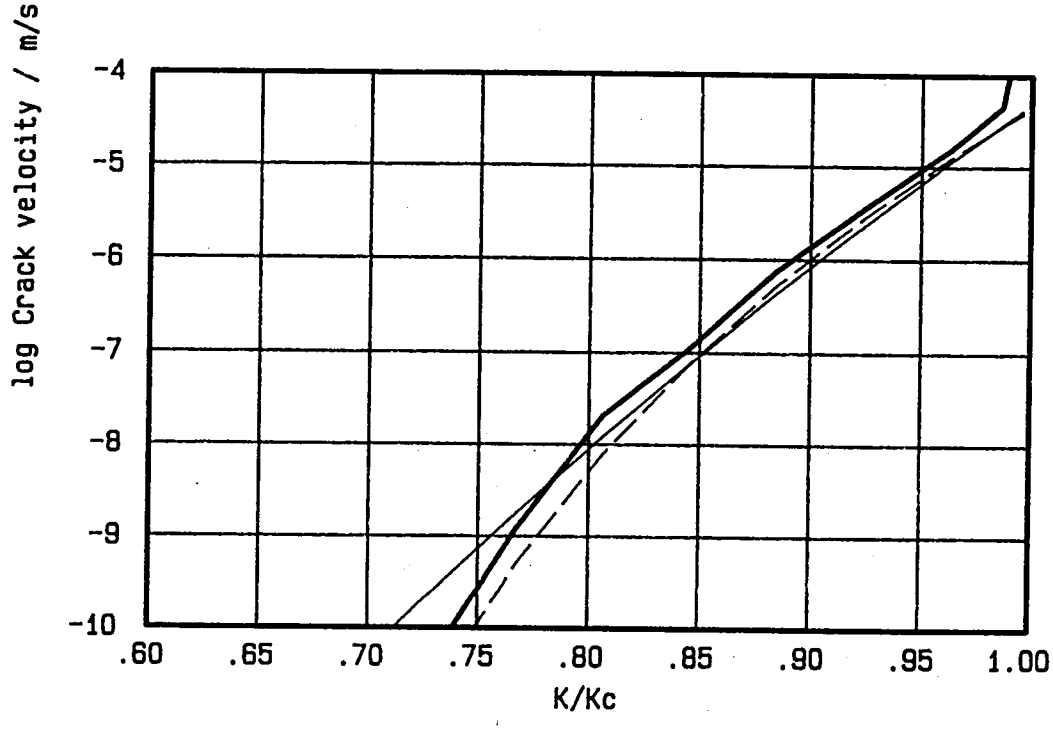

Figure 13. - Crack growth rate data.

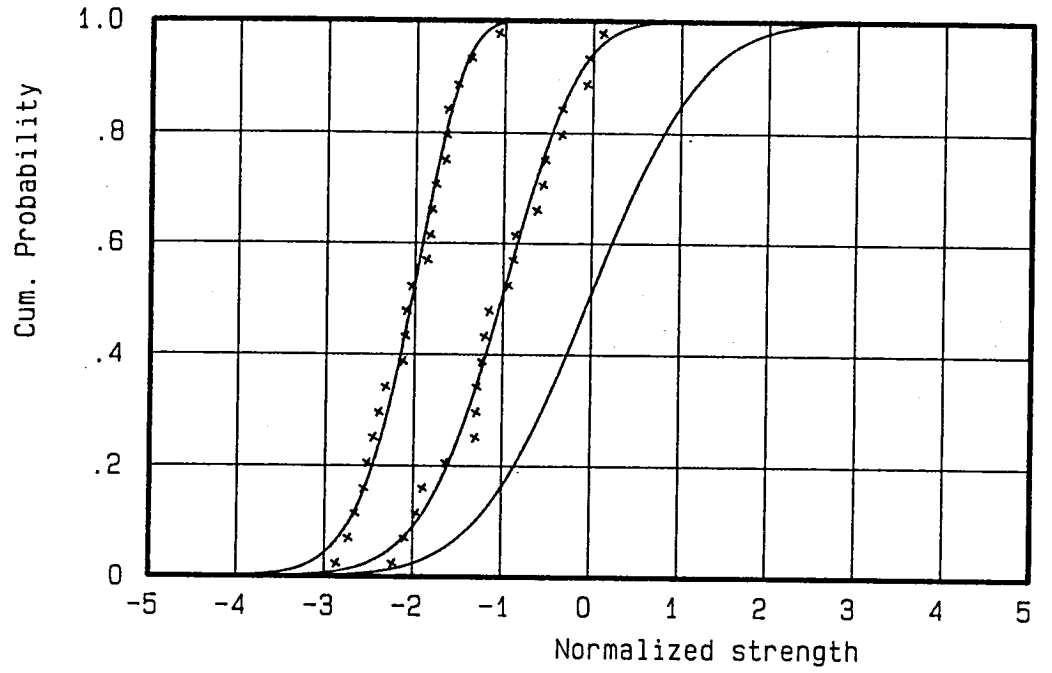

Figure 14. - Extreme value prediction and experimental data.

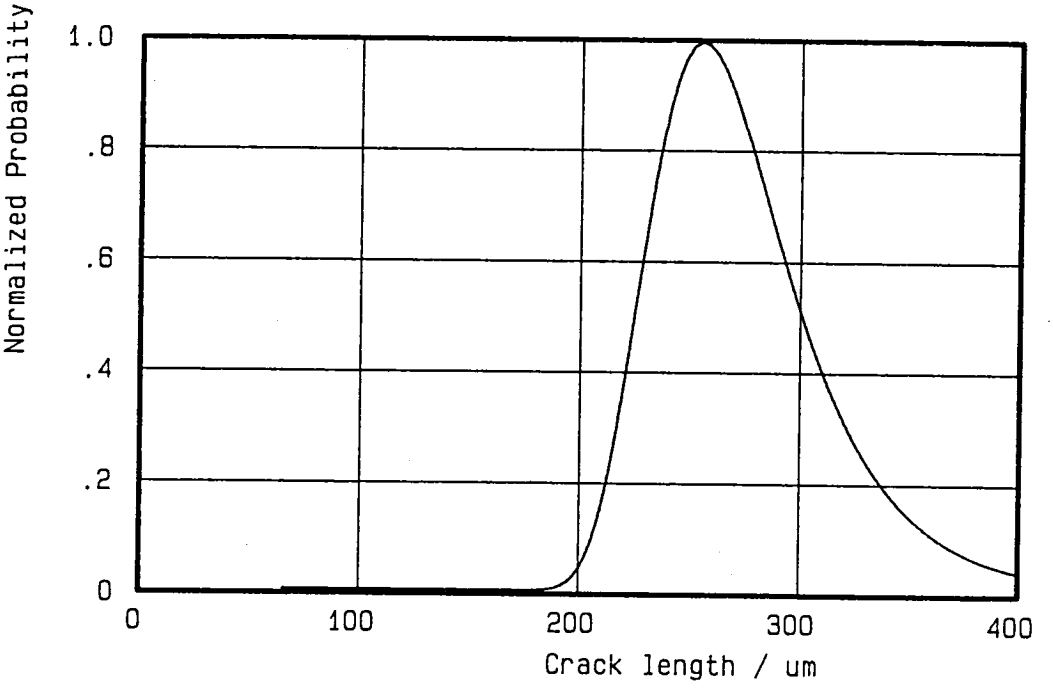

Figure 15. - Calculated distributions of initial crack length.

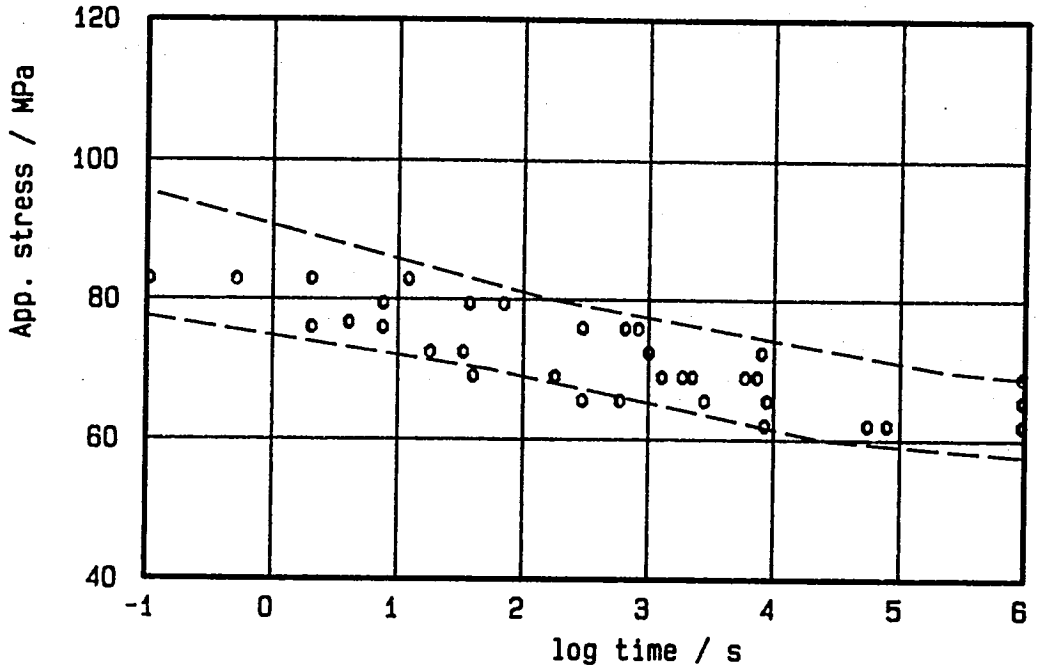

Figure 16. - Predicted 90% confidence band for 32 indentations.

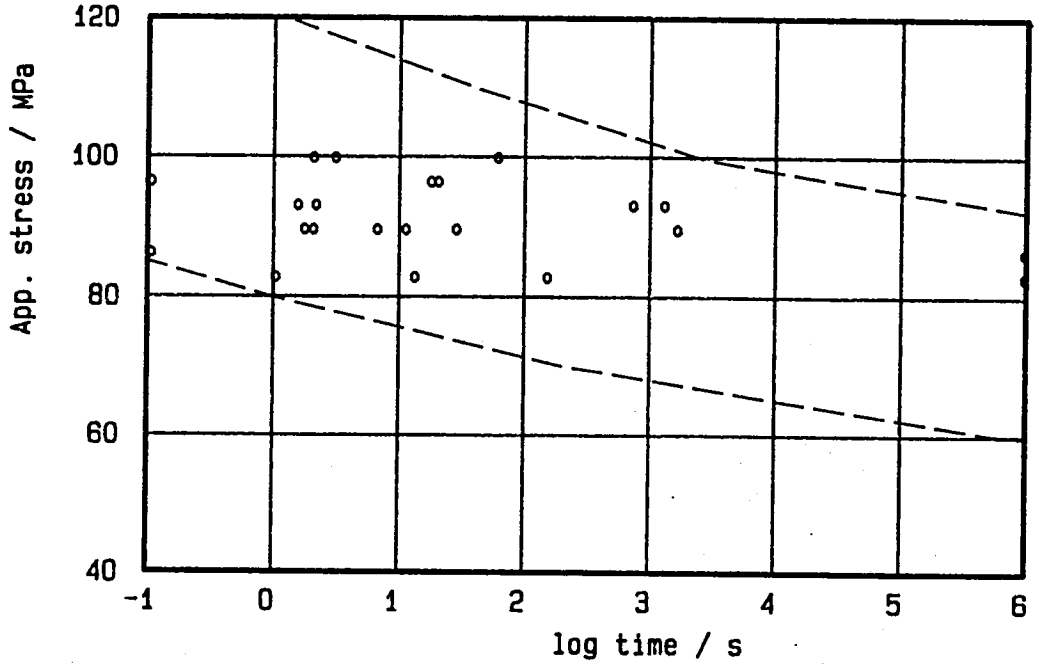

Figure 17. - Predicted 90% confidence band for 4 indentations.

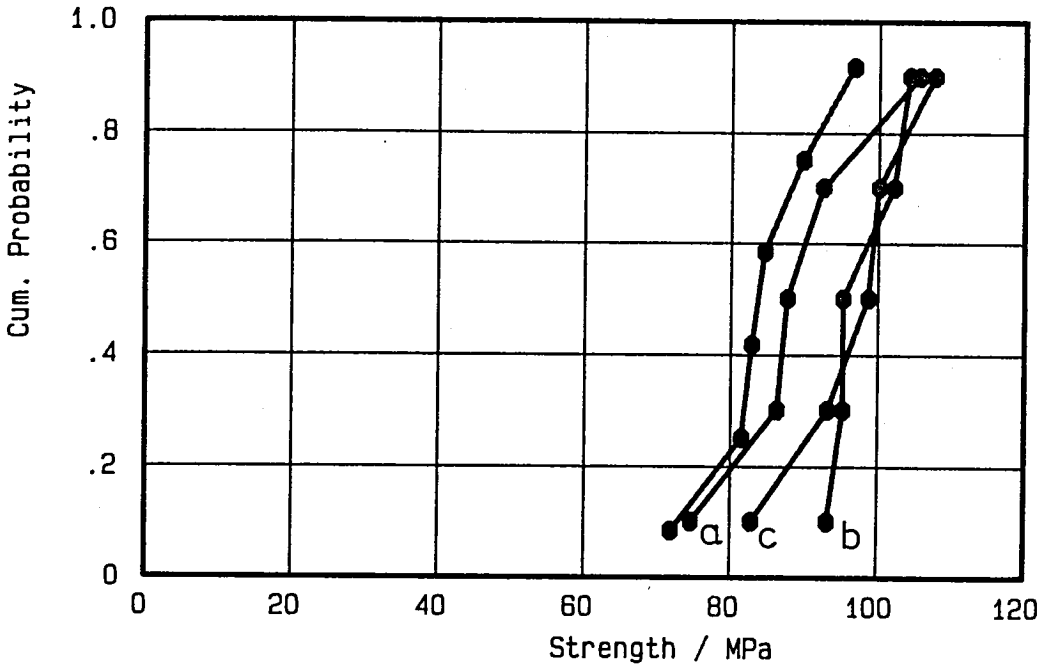

Figure 18. - Runout strength data.

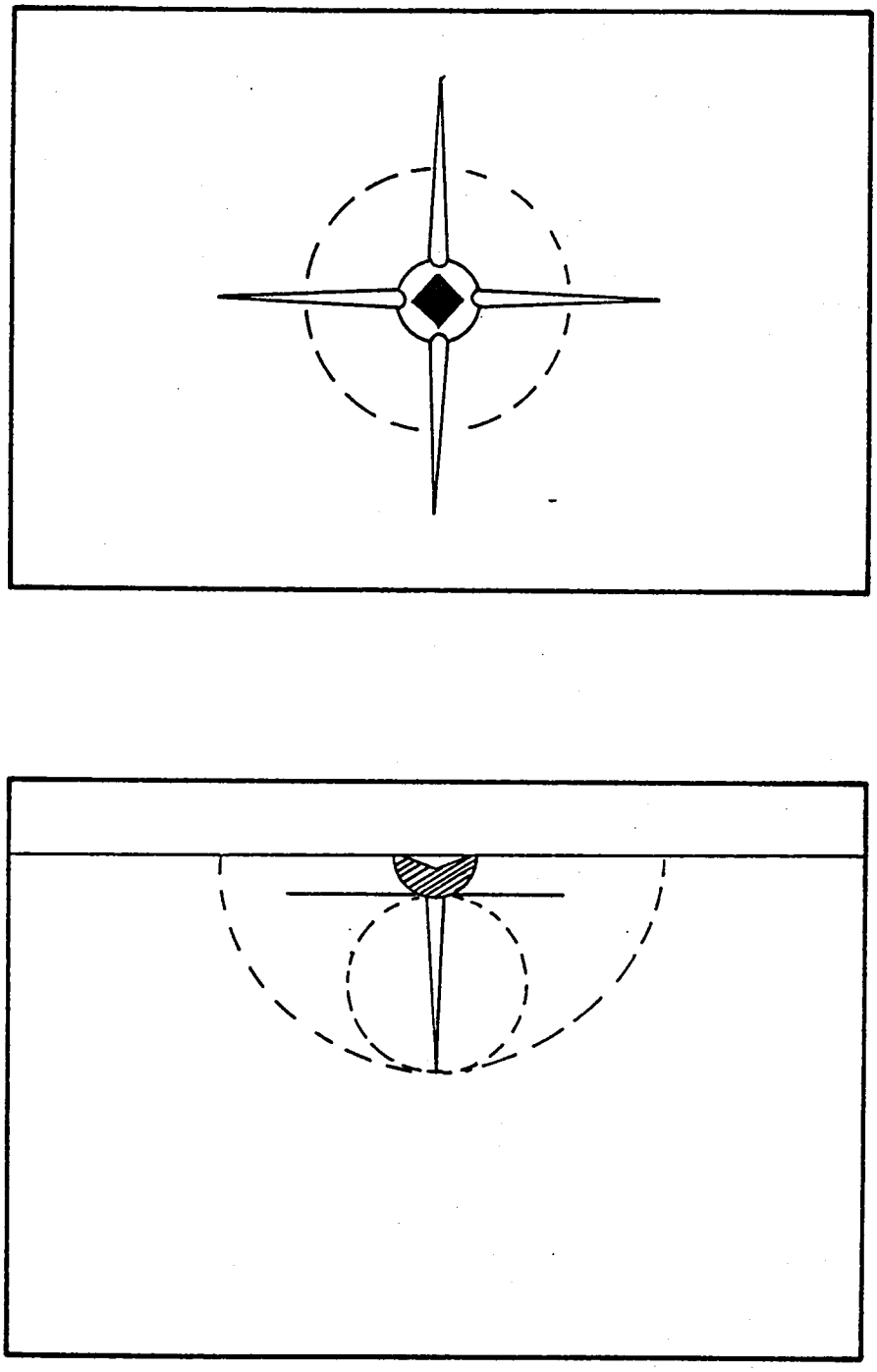

Figure A1.- Ideal indentation as observed in glass as an example.

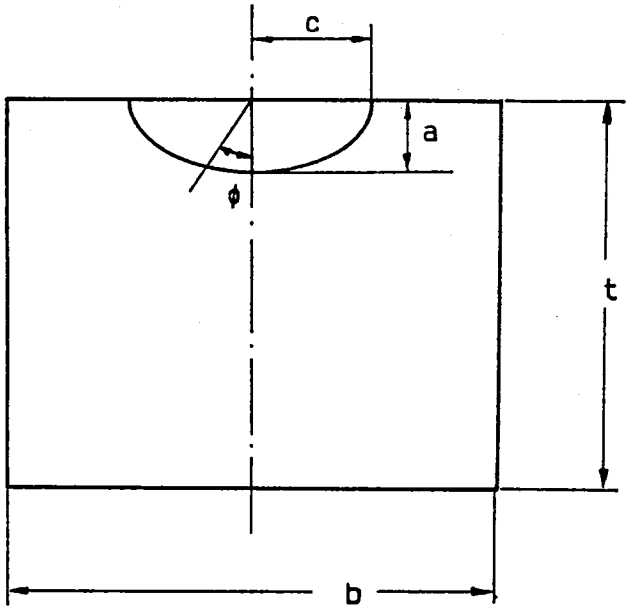

Figure B1. - Surface flaw, dimensions.

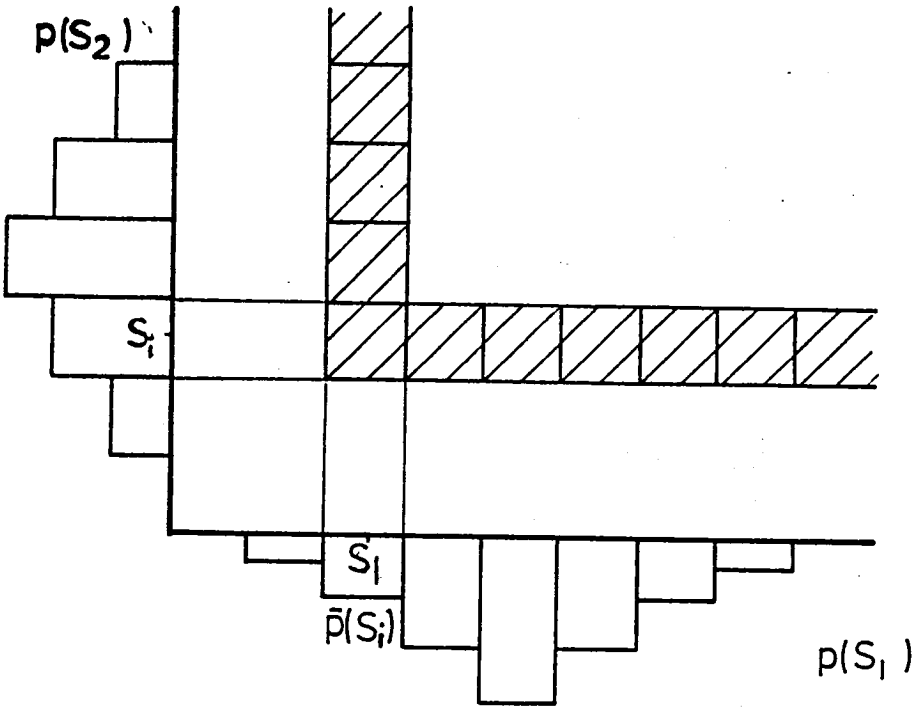

Figure C1. - Two dimensional probability domain.

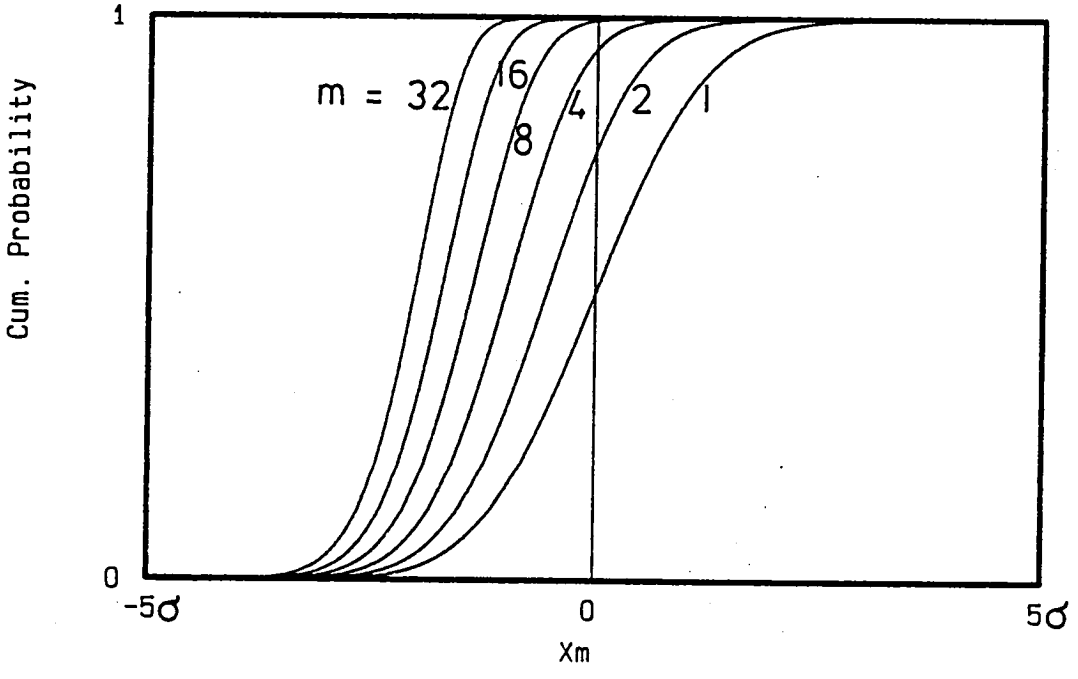

Figure C2. - Cumulative probability curves for m events.

1. Report No.	2. Government Accession No.	3. Recipient's Catalog No.
NASA TM-85644		

4. Title and Subtitle	5. Report Date
SLOW CRACK GROWTH IN SPINEL IN WATER	May 1983
	6. Performing Organization Code 534-03-23-05
7. Author(s) *Stephan Schwantes and Wolf Elber	8. Performing Organization Report No.
9. Performing Organization Name and Address NASA Langley Research Center Hampton, VA 23665	10. Work Unit No. 11. Contract or Grant No.
12. Sponsoring Agency Name and Address National Aeronautics and Space Administration Washington, DC 20546	13. Type of Report and Period Covered Technical Memorandum 14. Army Project No.

15. Supplementary Notes

*DAAD guest student, George Washington University.

16. Abstract

Magnesium aluminate spinel ($MgAl_2O_4$) was tested in a water environment at room temperature to establish its slow crack-growth behavior. Ring specimens with artificial flaws on the outside surface were loaded hydraulically on the inside surface. The time to failure was measured. Various precracking techniques were evaluated and multiple precracks were used to minimize the scatter in the static fatigue tests. Statistical analysis techniques were developed to determine the strength and crack velocities for a single flaw. Slow crack-growth rupture was observed at stress intensities as low as 70 percent of K_c. A strengthening effect was observed in specimens that had survived long-time static fatigue tests.

17. Key Words (Suggested by Author(s))	18. Distribution Statement
Ceramics Fracture mechanics Crack growth Statistical analysis Environmental testing	Unclassified - Unlimited Subject Category 27

19. Security Classif. (of this report)	20. Security Classif. (of this page)	21. No. of Pages	22. Price*
Unclassified	Unclassified	44	A03

*For sale by the National Technical Information Service, Springfield, Virginia 22161